J Solid State Electrochem (2011) 15:1159–1168
DOI 10.1007/s10008-010-1177-7

ORIGINAL PAPER

Electrodeposition of composite Ni–B coatings in a stirred heterogeneous system

Renáta Oriňáková · Katarína Rošáková · Andrej Oriňák · Miriam Kupková · Jean Nicolas Audinot · Henri-Noël Migeon · Jan T. Andersson · Karol Kovaľ

Received: 20 April 2010 / Revised: 9 August 2010 / Accepted: 10 August 2010 / Published online: 1 September 2010

Abstract The formation of composite electrochemical coatings of a nickel matrix with boron microparticles was investigated. Electrolytical nickel–boron layers were deposited on a paraffin-impregnated graphite electrode in a stirred heterogeneous system formed by a Watts-type nickel plating bath and dispersed boron powder particles. The polarisation behaviour of the composite plating bath as a function of the boron particle loading was examined. The effect of deposition conditions, as well as of the amount of boron powder in the plating bath on the boron content in the composite Ni–B coatings, was examined. The composite coating structure was established using scanning electron microscopy and light optical microscopy. The distribution of boron particles in the composite deposits was investigated by dynamic secondary ion mass spectrometry. The boron particles content was determined gravimetrically. The obtained results suggest that the content of incorporated boron particles increases with an increasing amount of boron in the plating bath. The potentiodynamic deposition method is demonstrated to be more suitable for production of composite coatings with a high content of boron particles than the potentiostatic one. Homogeneous distribution of boron particles in the nickel matrix without coagulation or sedimentation was associated with the electrochemical fabrication method in stirred heterogeneous systems.

Keywords Composite Ni–B coating · Stirred heterogeneous system · Potentiostatic deposition · Potentiodynamic deposition · Watts-type electrolyte

R. Oriňáková (✉) · K. Rošáková · A. Oriňák
Institute of Chemistry, Faculty of Science,
P.J.Šafárik University,
Moyzesova 11,
SK-04154 Košice,
Slovak Republic
e-mail: Renata.Orinakova@upjs.sk

M. Kupková · K. Kovaľ
Institute of Material Research,
Slovak Academy of Science,
Watsonova 47,
SK-04353 Košice, Slovak Republic

J. N. Audinot · H.-N. Migeon
Department of Science and Analysis of Materials,
Gabriel Lippmann Public Research Centre,
41, rue du Brill,
4422 Belvaux, Luxembourg

J. T. Andersson
Institute of Inorganic and Analytical Chemistry,
University of Münster,
Corrensstr. 30,
48149 Münster, Germany

Introduction

Electroplating is one of the few surface-finishing processes that can satisfy the requirements of decorative and functional applications and improve the operating properties of products subjected to external hazards. Nickel deposition has been widely studied, and much work has been devoted to the mechanism of the deposition process. The properties and structures of the electrodeposits are closely related to the electrolyte composition and electroplating parameters [1–3].

Introducing boron (B) into nickel matrixes enables one to obtain materials with high microhardness and significantly better wear resistance. Their mechanical and tribological properties are of great interest for industrial applications, especially in cases where high abrasive and protective properties are required, for instance in the aerospace, automotive, electronic, and chemical industries [4, 5].

Another potential application of Ni–B coatings is the substitution of noble metals in the semiconductors and printed circuits boards [6].

Since the discovery of autocatalytic electroless nickel plating by Brenner and Riddel in 1946, its use has continuously grown because of the useful combination of properties and characteristics of the product [4]. Electroless Ni–B coatings are more wear-resistant than tool steel and hard chromium coatings and have an excellent solderability [7]. A few papers have reported on the effect of the bath composition and the deposition parameters on the amount of boron in the electroless Ni–B films [8, 9]. Electroless deposition is carried out by using strong reducing agents such as borohydride, hydrazine borane, pyridine borane and dimethylamine borane [10]. Properties of Ni–B films are influenced particularly by their boron content [8–10]. The microstructural and thus the mechanical properties of Ni–B films are significantly affected by heat treatment [8, 11].

Moreover, Ni–B alloys can be produced by electrodeposition applying the above-mentioned reducing agents [10]. The electrochemical Ni–B alloy coating was achieved by Lee et al. [10]. The composition of the nanocrystalline Ni–B films, structural features and phase transformation of Ni–B before and after heat treatment, and their relation with internal stress, microhardness and wear properties were investigated. The internal stress was tensile and increased linearly with increasing boron content as did the hardness of Ni–B films. On the contrary, the wear resistance decreased with increasing boron content. A nickel–boron-based ethanol sensor was constructed by Y-Ch. Weng et al. [12]. The nickel–boron electrode electrodeposited using the thin film technique from a Watts-type electrolyte exhibited good electrochemical performance in terms of response time, linearity and sensitivity. This sensor also showed a high selectivity to ethanol.

The electrodeposition technique can also be used for the production of composite layers with a nickel matrix [6]. The nano- or micro-sized particles, suspended in the electrolyte by agitation and/or through the use of surfactants, can be co-deposited with the metal or polymer to produce the composite coatings. Introduction of solid particles into a metallic or polymeric matrix results in a modified material with enhanced mechanical, corrosion, electrocatalytic and tribological properties. The embedded particles can be selected to fulfil specific mechanical, electrical, piezoelectrical or magnetic properties in thin coatings [13–15]. Nickel, being an engineering material, is a widely used metal matrix.

Electroplated Ni–B composite coatings are reported by Gajewska-Midzialek and co-workers [6]. The wear resistance and microhardness of coatings were defined depending on the bath composition and boron content. Nickel–boron composite coatings were obtained by electroplating nickel from a bath containing dispersed boron particles by I. Rajagopal [16]. This deposit formed Ni–Ni_3B and Ni–Ni_2B composites after heating to 300 °C and 400 °C, respectively. Mechanical properties, corrosion resistance and wear resistance of the composites were better than nickel or the electroless Ni–B composite in the as-deposited condition. Production of composite Ni–B electrodeposits with a uniform distribution of boron particles throughout their matrix was demonstrated also by Fedorchenko et al. [17]. It was observed that the diffusional annealing led to the formation of qualitatively new structures in such deposits and improved their physicomechanical characteristics. The wear resistance of heat-treated Ni–B deposits was as high as that of hard chromium electrodeposits. Medeliene et al. have deposited Ni–B coatings from an electrolyte containing saccharine [18]. The corrosion resistance, microstructure, mechanical and physical properties of the deposits were investigated. The non-metallic inclusions on the surface of Ni–B coating layer affected the corrosion behaviour of the coating as well as its mechanical and physical properties.

The purpose of the present work was to produce Ni–B composite coatings by electrochemical co-deposition of boron microparticles with nickel, from an additive-free Watts-type bath. Electrodeposition was carried out under potentiostatic and potentiodynamic conditions in stirred heterogeneous systems with the aim to evaluate the effect of operating parameters that influence the quantity of micro-sized boron particles incorporated into the nickel deposit such as scan rate, deposition potential and amount of boron particles suspended in the plating bath. The surface morphology of the deposits was investigated along with the distribution and the percentage of the embedded microparticles in the nickel matrix affected by the electrodeposition parameters.

Experimental

The electrodeposition of composite Ni–B coatings was carried out using a Watts nickel plating electrolyte of following composition: 1.2 $molL^{-1}$ $NiSO_4.7\ H_2O$, 0.6 $molL^{-1}$ NaCl, and 0.6 $molL^{-1}$ H_3BO_3 (pH=2.00±0.02). Crystalline boron powder particles (size, less than 40 μm) of Sigma–Aldrich production in concentration of 2, 6 or 8 gL^{-1} were used as the dispersion particles. The electroplating was realised (1) potentiodynamically in the potential range from −350 mV to −1,500 mV (three cycles) with polarisation rates: 1 mVs^{-1}; 12.5 mVs^{-1}; 25 mVs^{-1}; and 50 mVs^{-1}, as well as (2) potentiostatically at potentials of −900 mV or −1,000 mV with a duration of 10 min, at room temperature with mechanical stirring at 300 rpm.

All cyclic voltammetry experiments were carried out with an EcaStat potentiostat/galvanostat, model 110 V (Istran, Slovak Republic). The electrochemical cell con-

sisted of a classical 3-electrode set-up with an Ag/AgCl (3 $molL^{-1}$ KCl) electrode as the reference electrode, a platinum sheet as the counter electrode and a paraffin-impregnated graphite electrode (PIGE) as the working electrode. The current was normalised per geometric PIGE surface area (0.283 cm^2). To obtain reproducible results, the surface of the PIGE was mechanically renewed with emery paper, polished on glossy paper, then washed with distilled water and degreased with acetone.

The main argument for application of this electrode was the possibility to achieve good reproducibility of the surface in contrast to the bad reproducibility of some metallic electrode surfaces. Thus, the reproducibility of voltammetric measurements consisted especially in the relatively constant background current corresponding to almost constant electrode surface area. Further advantages of PIGE are: simple preparation, easy renewal of the surface and reasonable price.

Dispersed phase content in the coating was determined gravimetrically with coating dissolution in nitric acid diluted 1:1 with water.

Microscopic observations of Ni and Ni–B films were made using a scanning electron microscope (SEM, Tesla BS 340) and light optical microscope (LOM, Neophot 32). Compacted cylindrical samples prepared from iron particles (water-atomized iron powder, Höganäs, ASC 100.29 grade of size fraction 63–200 μm) were coated with bare Ni or composite Ni–B layer and were thereafter cross-sectioned for metallographic examination, mounted, ground, and polished using well-established practises. To obtain adherent coatings, the surface of iron cylinders was chemically activated prior to the coating deposition, involving degreasing by etching in 10% aqueous solution of hydrazinium dihydrochloride for a period of 5 min, then rinsing with distilled water and acetone.

The elemental distribution of boron particles was imaged by means of dynamic secondary ion mass spectrometry (DCameca NanoSIMS50). NanoSIMS50 maps were acquired under standard analytical conditions: a Cs^+-ion primary beam with impact energy of 16 keV, and a current of 1 pA was used. Under these conditions, a lateral resolution below 70 nm can be expected. The raster area was 30×30 μm^2 for an image of 256×256 pixels. The parallel detection of secondary negative ions ^{11}B, ^{12}C, ^{16}O, ^{28}Si, and ^{58}Ni was done in the multicollection mode. The mass resolution obtained was about $M/\Delta M$=5,000.

Results and discussion

Solid crystalline boron powder particles were dispersed by mechanical stirring of the electrolyte. With a sufficiently high stirring rate, the whole bed of particles was maintained in a suspended state so that the dispersed particles come intermittently into contact with a solid electrode surface. A fraction of them was captured on the electrode surface where the nickel deposition proceeded, becoming thereby embedded in the nickel matrix.

Cyclic polarisation curves

The mechanism of Ni deposition has been demonstrated to depend on a number of factors, such as pH, concentration, electrode material and bath additives. Several authors [19–22] assume that the nickel reduction most likely occurs through the nickel hydroxo ions, $Ni(OH)^+$. The formation of the electroactive species supports a local increase in pH near the deposit/electrolyte interface due to hydrogen evolution. The probable mechanism can be expressed as a sequence of reactions:

$$Ni^{2+} + H_2O \rightleftarrows NiOH^+ + H^+ \quad (1)$$

$$NiOH^+ \rightarrow NiOH^+_{ads} \quad (2)$$

$$NiOH^+_{ads} + e^- \rightarrow NiOH_{ads} \quad (3)$$

$$NiOH_{ads} + H^+ + e^- \rightarrow Ni + H_2O \quad (4)$$

The electroplating of nickel proceeds simultaneously with the hydrogen discharge reaction. In the course of this process, atomic hydrogen is formed and adsorbed on the electrode surface covered by deposited nickel. The overall reaction may be described by a combination of the following steps:

$$Ni + H^+ + e^- \rightarrow Ni - H_{ads} \quad (5)$$

$$2Ni - H_{ads} \rightarrow 2Ni + H_2 \quad (6)$$

$$Ni - H_{ads} + H^+ + e^- \rightarrow Ni + H_2 \quad (7)$$

The formation of two interstitial hydrogen alloys of nickel during the electrodeposition has been reported [23, 24]. α-Nickel is a solid solution, which has an atomic ratio H/Ni less than 0.03. Its electrodeposition appears to follow the laws for progressive nucleation and 3-dimensional growth [23, 24]. β-Nickel (nickel hydride β phase) has the atomic ratio between 0.6 and 1.0. It is predominantly originated in the early stages of deposition, and its deposition appears to be restricted by mass transfer of hydrogen ions. Formation of β-nickel is accelerated at low pH and higher negative potentials [23, 24].

The cyclic voltammograms for the Watts electrolyte and Watts electrolyte with boron particles recorded on PIGE are shown in Fig. 1. A sharp current increase starting at about −700 mV was registered. The observed rapid cathodic current increase on the polarisation curve corresponds to

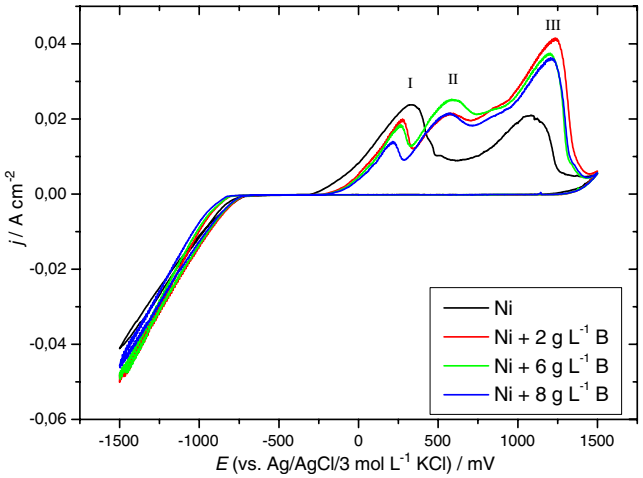

Fig. 1 Polarisation curves for a bare nickel layer and the composite Ni–B layers electrodeposition from Watts electrolyte: 1.2 molL^{-1} $NiSO_4$.7 H_2O, 0.6 molL^{-1} NaCl, 0.6 molL^{-1} H_3BO_3 (pH = 2 ± 0.02) on PIGE depending on B microparticle loading. The polarisation rate was 12.5 mVs^{-1} and the rate of stirring was 300 rpm. The working electrode was polarised in the potential range from 0 V to −1.5 V, than to +1.5 V and back to 0 V (vs. Ag/AgCl (3 molL^{-1} KCl))

the potential at which Ni starts to nucleate. The hydrogen evolution commences simultaneously with the nickel electrodeposition with a further shift to more negative potentials. It is seen that the addition of B particles to the Watts electrolyte causes the reduction potential of Ni to shift towards more negative values, see also Fig. 2. The shift of the metal ion reduction is probably explained by the boron microparticles colliding with the cathode, thus hindering the metal deposition. The dispersed B phase changes the slope of the cathodic polarisation curves during nickel electroplating but does not alter their shape significantly.

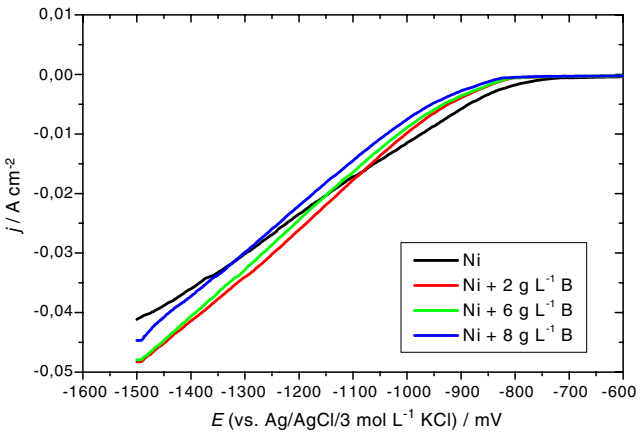

Fig. 2 Cathodic polarisation curves for composite Ni–B layers electrodeposition from Watts electrolyte:1.2 molL^{-1} $NiSO_4$.7 H_2O, 0.6 molL^{-1} NaCl, 0.6 molL^{-1} H_3BO_3 (pH = 2 ± 0.02) on PIGE depending on B microparticle loading. The polarisation rate was 12.5 mVs^{-1}, and the rate of stirring, 300 rpm. The working electrode was polarised in the potential range from 0 V to −1.5 V, than to +1.5 V and back to 0 V (vs. Ag/AgCl (3 molL^{-1} KCl))

The anodic part of the polarisation curves corresponds to the dissolution of deposited metallic layer. Two separated oxidation peaks were observed for dissolution of Ni at about 330 mV (I) and 1,120 mV (III) and probably may be assigned to the oxidation of β-nickel and α-nickel, respectively, as was indicated previously [23–26]. It should be noted that no additional experiments were performed to approve this rough assumption, and observed peaks could be differently interpreted. Besides the two oxidation peaks mentioned at nearly similar position, one further oxidation peak at about 600 mV (II) was observed for the dissolution of the composite Ni–B film. The oxidation peak corresponding to the oxidation of β-nickel (I) decreased, while the oxidation peak corresponding to the α-nickel oxidation (III) increased with an increasing amount of boron microparticles in the plating electrolyte. Moreover, the overall area of the anodic peaks increases with an increasing amount of B particles, indicating the higher amount of deposited coating layer.

Figure 2 shows the cathodic polarisation curves of the Ni plating electrolytes containing different concentrations of B microparticles. It is found that the introduction of B causes an increase in the cathodic polarisation. The experimental deposition potentials (corresponding to the current density 0.7 mAcm^{-2}) of metals on PIGE versus the Ag/AgCl (3 molL^{-1} KCl) electrode for different contents of boron particles are listed in Table 1. The shift to a more negative value in the reduction potential may be attributed to a decrease in the active surface area of the cathode, owing to the adsorption of boron microparticles, and may also be related to the decrease in the ionic transport by the B particles [27, 28]. It is also evident from Figs. 1 and 2 that with the shift to more negative potentials the cathodic current of the composite films deposition exceeds that of the bare nickel deposition. Moreover, the reduction of H^+ would occur more quickly than the reduction of Ni^{2+} when the overpotential is increasing. Changes in the slopes of the cathodic part of the curves and also the higher cathodic current at the switching potential (−1.5 V) reflect an acceleration in the deposition rate of composite Ni–B films with increasing overpotential. This is accompanied by an

Table 1 Values of the experimental deposition potentials of Ni and composite Ni–B films on PIGE versus Ag/AgCl (3 molL^{-1} KCl) electrode corresponding to the current density of 0.7 mAcm^{-2} as a function of the boron particle loading

Concentration of B in bath/gL^{-1}	Deposition potential/mV
0	−734
2	−810
6	−813
8	−830

increase in the α-nickel along with a decrease in the β-nickel content in the deposited films.

From the results obtained, it may be concluded that at a low overpotential (nickel reduction potential) boron particles hinders the nucleation of nickel and thus the deposition of composite films. However, at higher overpotential (hydrogen evolution potential), the presence of boron together with hydrogen evolution enhances the composite film deposition and leads to an increase in the quantity of α-nickel hydride. The observed results may be a consequence of the diverse influences of boron particles on the nucleation and growth process of nickel deposition and of the hydrogenation effect at more negative potentials.

The appropriate potentials for potentiostatic deposition have been selected from the cathodic polarisation curves.

Effect of particle loading on embedded particle content

The B content in the composite Ni–B deposits is very important because it allows easy control of the physical and mechanical properties such as density, hardness, stress, and melting point. Generally, a higher level of B in the coating is responsible for the major improvement in properties.

The weight percentage of B particles in composite Ni–B deposits produced from the processes discussed as a function of particle loadings ranged from 3.6 to 22.2 wt%. The dependence of boron particles and nickel content in composite Ni–B coating on the concentration of boron microparticles in the plating bath and on the plating conditions is presented in Fig. 3a and b, respectively. The solid lines reflect the general trends. The percentage content (Fig. 3a) of boron particles incorporated into the composite Ni–B deposits increases with an increasing amount of boron microparticles suspended in the plating bath. The increase seems to be nearly linear, but there is an indication of a levelling off at higher boron content. The amount of particles co-deposited can be correlated with a chance entrapment of the particles [29]. On the contrary, the content of nickel (Fig. 3b) in composite films decreased with an increasing concentration of boron in the electrolyte. The highest boron content was registered for the potentiodynamic deposition method at a scan rate of 12.5 mVs^{-1}. The content of boron in the composite layer in this case ranged from 14.9 to 22.2 wt% depending on the amount of boron in the plating bath. The boron content in the deposits prepared under the remaining conditions was at least 5 wt% lower. The lowest content of boron was observed at the slowest scan rate (1 mVs^{-1}) as well as for the potentiostatic deposition at a potential of −900 mV, conditions that led to high amounts of nickel in the composite coatings under the mentioned conditions.

From these results, it may be concluded that the potentiodynamic deposition is more appropriate for composite Ni–B coating deposition than the potentiostatic one.

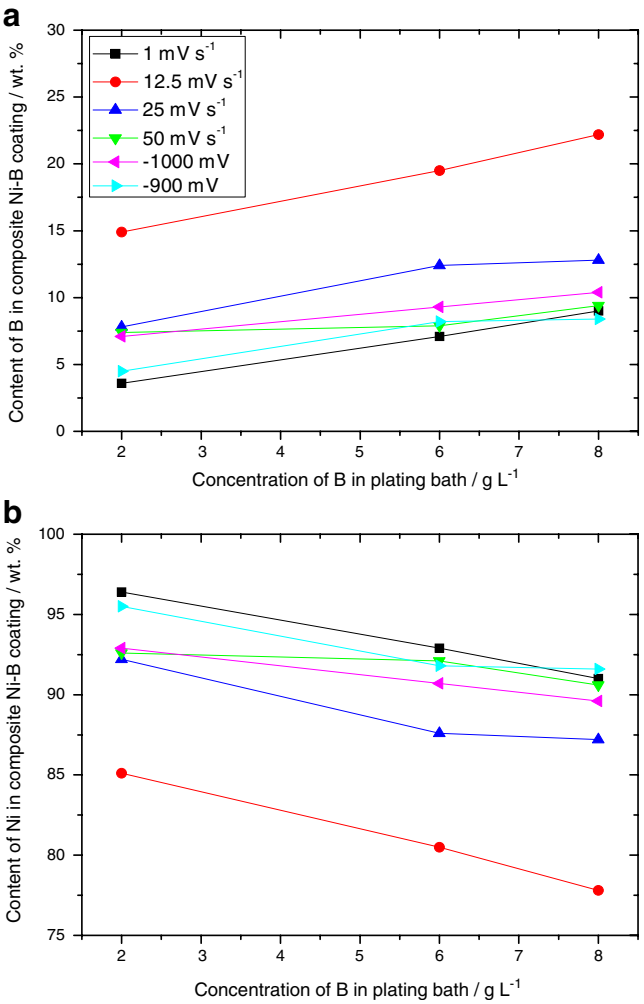

Fig. 3 Content of B (**a**) and Ni (**b**) (in wt%) in the composite Ni–B coating layer as a function of suspended boron microparticles concentration in the plating bath for different deposition conditions

The more desirable scan rate for electrolytical deposition of composite Ni–B film, in the view of high boron content, is 12.5 mVs^{-1}.

Distribution of boron particles in composite Ni–B coatings

The distribution of nickel and boron over the surface of the composite deposits was examined by means of secondary ion mass spectrometry (SIMS) mapping analysis. Pure Ni deposits were also produced under the same experimental conditions and examined as the reference state for comparison.

NanoSIMS50 images of bare Ni and composite Ni–B coatings produced potentiodynamically using a potential scanned between −350 mV and −1,500 mV at a scan rate of 25 mVs^{-1} are given in Figs. 4 and 5. The scale of colour goes from black to red with increasing intensity. Recorded masses were: ^{11}B, ^{12}C, ^{16}O, $^{12}C^{14}N$ or ^{28}Si and ^{58}Ni. ^{28}Si has been chosen for the bare Ni sample (Fig. 4) due to the

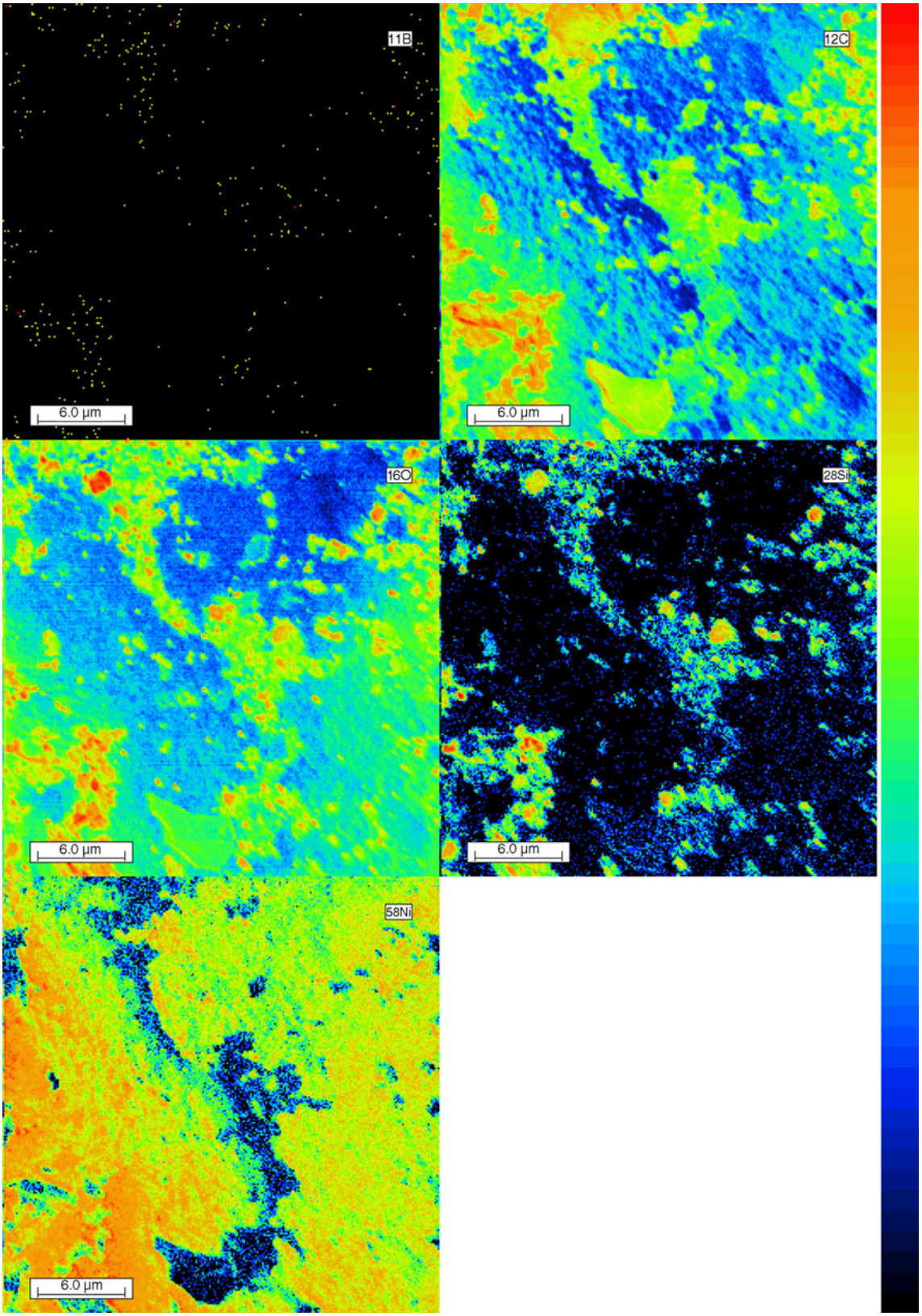

Fig. 4 SIMS maps of elemental distributions of ^{11}B, ^{12}C ^{16}O, ^{28}Si, and ^{58}Ni on sample Ni produced potentiodynamically by scanning the potential between −350 mV and −1,500 mV at scan rate 25 mVs^{-1}. The scale of colour goes from black to red with increasing intensity. Field of view, 30×30 μm^2; acquisition time, 25 ms/pixel; logarithmic scale

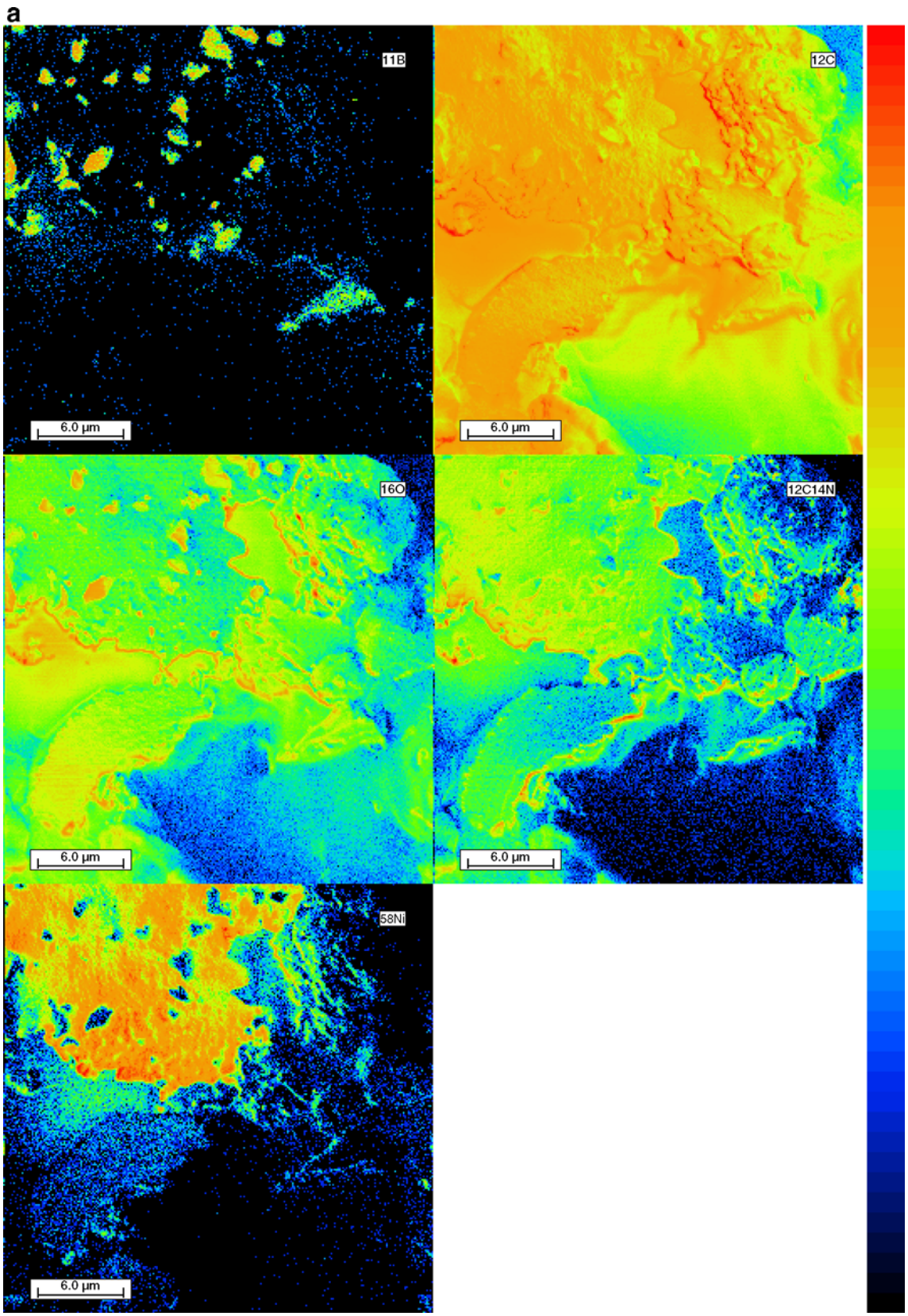

Fig. 5 SIMS maps of elemental distribution of ^{11}B, ^{12}C ^{16}O, $^{12}C^{14}N$, and ^{58}Ni on sample Ni–B produced potentiodynamically by scanning the potential between −350 mV and −1,500 mV at scan rate 25 mV s^{-1} (**a**). Field of view, 30×30 µm^2; acquisition time, 30 ms/pixel; logarithmic scale (**b**). Superposition of the SIMS images of ^{11}B (*blue*) and ^{58}Ni (*red*)

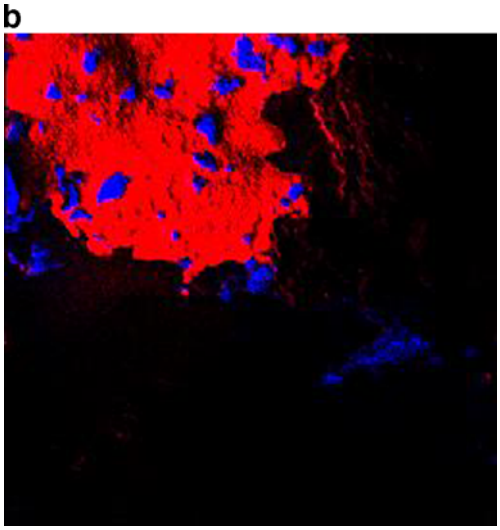

Fig. 5 (continued)

preparation of the sample. The electrodeposited film was peeled off from the carbon electrode and then placed on a silicon wafer, so a hole in the film would be detected by the presence of silicon.

The nodular structure of the nickel deposit can be seen from SIMS image in Fig. 4. In consequence of the fast potential shift, the deposited layer was thin and not compact. SIMS mapping analysis of the nickel deposit revealed, in addition to the known constituents of the coating and substrate material (Ni, C, Si, and O), the presence of boron, too. The detected traces of boron apparently arise from the electrolyte solution containing boric acid. The surface morphology of the nickel matrix in composite Ni–B coating (Fig. 5a) is identical, but the deposit is even less coherent, and it covered a smaller field of the electrode surface. Some inhibition of nickel deposition in the presence of boron particles was registered. SIMS maps clearly show the regular distribution of boron particles built into the nickel matrix without formation of aggregates (Fig. 5a). This finding is proved also by Fig. 5b in which the superposition of images of boron and nickel is presented. By visualisation of boron and nickel this analysis allows for exact location of boron particles on the surface of the composite film. Individual boron microparticles (blue) are dispersed throughout the whole surface of the Ni matrix (red). Several particles were detected on the electrode surface in the vicinity of the composite deposit. A few maps were taken from different places on the film surface to express the relevant distribution. The observed homogeneous distribution originated from an electrolytical deposition method in stirred heterogeneous system with intensive agitation of the suspension and consecutive formation of the composite film by coating of incorporated boron particles with an incipient nickel layer.

Surface morphology of composite Ni–B coatings

SIMS analysis has been supplemented with the information obtained from SEM and LOM analysis. SEM images of the Ni–B surfaces plated potentiodynamically and potentiostatically under different experimental conditions are presented in Figs. 6 and 7, respectively, for a boron amount in the plating bath of 8 gL^{-1}. It can be seen that the Ni–B composite coating develops a nodular surface structure. The

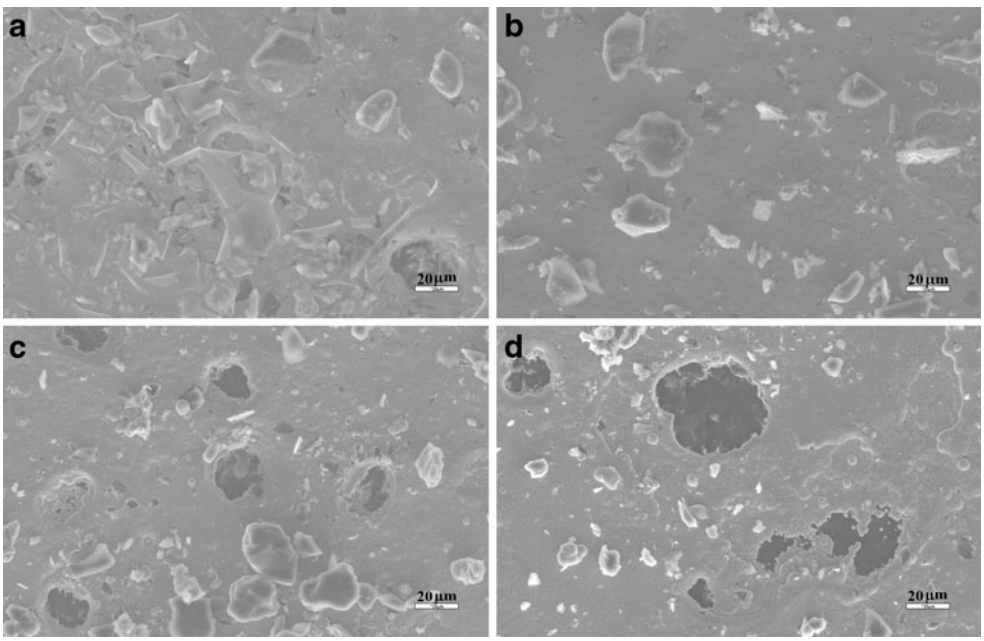

Fig. 6 Scanning electron micrographs of surface of composite Ni–B layers produced potentiodynamically from Watts electrolyte with 0.4 g of boron microparticles with potential scanned between −350 mV and −1,500 mV at 1 mVs^{-1} (**a**); 12.5 mVs^{-1} (**b**); 25 mVs^{-1} (**c**), and 50 mVs^{-1} (**d**) on PIGE at room temperature with rate of mechanical stirring of 300 rpm. The length of the white line scale in the right corner of the images represents the value of 20 µm

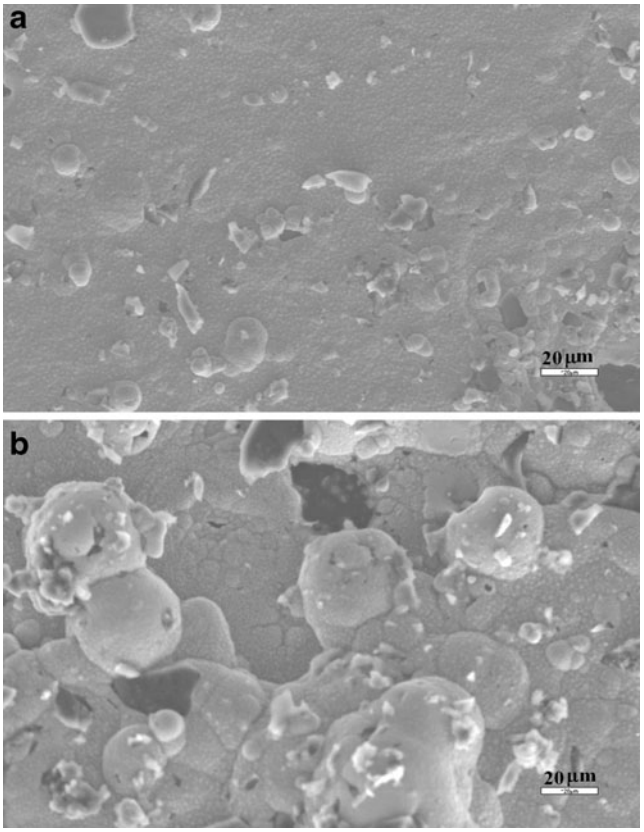

Fig. 7 Scanning electron micrographs of surface of composite Ni–B layers produced potentiostatically from Watts electrolyte with 8 gL^{-1} of boron microparticles at −900 mV (**a**) and −1,000 mV (**b**) on PIGE with duration of 10 min, at room temperature with rate of mechanical stirring of 300 rpm. The length of the white line scale in the right corner of the images represents the value of 20 µm

nodule size increases with an increasing scan rate as was observed for Ni–B deposits. The deposited films became thinner and more incoherent with a shortened deposition time (Fig 6a, b). However, the coating layer appeared thick, cracked and scaled at the smallest scan rate. The presence of cracks indicates that the deposits are highly stressed due to the hydrogen evolution during electrodeposition. The simultaneous hydrogen evolution was evident from the dark circles sporadically created by hydrogen bubbles growing on the electrode surface (Fig. 6c, d).

In case of potentiostatic deposition, the more uniform, coherent and homogeneous deposits with smaller nodules were obtained at −900 mV (Fig. 7a). Films prepared at −1,000 mV (Fig. 7b) were rough, less homogeneous and characterised by a surface morphology affected by simultaneous hydrogen evolution. In addition, the nodule size of the Ni–B layer slightly decreased, and the nodule number increased with increasing content of boron in the composite deposits (not illustrated).

Figure 8 shows the cross-sectional LOM images of the interfaces between the iron substrate and the Ni deposit (Fig. 8a) and the composite Ni–B layer (Fig. 8b) produced potentiodynamically from a Watts electrolyte with 8 gL^{-1} of boron microparticles. The coatings possessed good adhesion to the iron substrate surface. The distribution of boron particles in the composite film appears uniform and level without agglomeration of embedded boron microparticles. Boron particles were superimposed by a growing nickel film during the electrolytical deposition and thereby incorporated in the bulk of the composite layer likewise on its surface. Boron particles embedded inside of the composite films give rise to its enhanced mechanical properties.

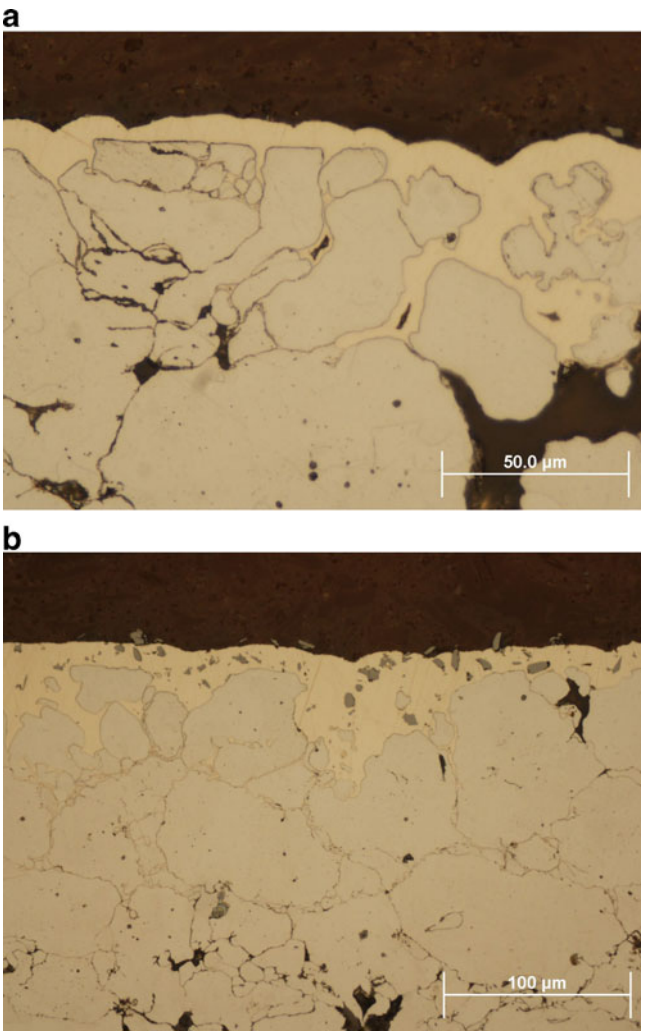

Fig. 8 Optical micrographs of cross-sections of cylindrical samples prepared from iron particles coated with bare Ni (**a**) and composite Ni–B layer (**b**) produced potentiodynamically from Watts electrolyte with 8 gL^{-1} of boron microparticles by scanning the potential between −350 mV and −1,500 mV at 12.5 mVs^{-1} at room temperature with rate of mechanical stirring of 300 rpm

Conclusions

In this study, Ni matrix composite films containing boron microparticles were produced by electrolytical deposition from additive-free nickel Watts-type plating baths. The effect of the boron microparticle loading on the electrodeposition of composite coatings was studied by means of cyclic voltammetry. The slight shift of deposition potential to more negative values and the higher cathodic current for deposition of composite Ni–B layer on PIGE was detected from cyclic polarisation curves. Boron particles adsorbed on the cathode hindered the reduction of metal ions owing to a decrease of the active surface area of the cathode, and thus caused an increase in cathodic polarisation. Rate of the composite film deposition increased with the concentration of boron particles as well by potential scanning to more negative values and led to an increase in the α-nickel content in the deposits.

Electrodeposition of Ni–B composites was carried out on PIGE by means of both potentiostatic and potentiodynamic methods in order to study the effect of electroplating parameters—such as scan rate, deposition potential and amount of boron microparticles in the plating bath—on the content of boron in composite deposits. The distribution and percentage of the embedded particles along with the structure and the surface appearance of the produced composite coatings were examined.

The feasibility to produce the composite Ni–B electrodeposits in a stirred heterogeneous system with a regular distribution of boron particles was demonstrated. The potentiodynamic deposition method was found to be more appropriate to obtain the composite coatings with high boron particle content than the potentiostatic deposition. The highest boron content was achieved at the scan rate 12.5 $mV s^{-1}$. The composite layers exhibited a nodular feature. Dynamic SIMS and LOM analyses revealed a homogeneous distribution of boron particles within and on the surface of composite films which resulted from the deposition process in a stirred heterogeneous system.

Acknowledgements Financial support from the Slovak Grant Agency VEGA under project No.1/0043/08 is gratefully acknowledged.

References

1. Landolt D (2002) J Electrochem Soc 149:S9
2. DiBari GA (1986) Metal Finish 84:23
3. Heusler E, Gaiser L (1968) Electrochim Acta 13:59
4. Vitry V, Delaunois F, Dumortier C (2008) Surf Coat Technol 202:3316
5. Riddle YW, Bailer TO (2005) JOM 57:40
6. Gajewska-Midzialek A, Szeptycka B, Derewnicka D, Nakonieczny A (2006) Tribol Int 39:763
7. Yoon JW, Koo JM, Kim JW, Ha SS, Noh BI, Lee ChY, Park JH (2008) J Alloy Comp 466:73
8. Anik M, Körpe E, Sen E (2008) Surf Coat Technol 202:1718
9. Delaunois F, Petitjean JP, Lienard P, Jacob-Duliere M (2000) Surf Coat Technol 124:201
10. Lee KH, Chang D, Kwon SC (2005) Electrochim Acta 50:4538
11. Krishnaveni K, Sankara Narayanan TSN, Seshadri SK (2005) Surf Coat Technol 190:115
12. Weng YCh, Chou TCh (2006) J Electrochem Soc 153:H127
13. Low CTJ, Wills RGA, Walsh FC (2006) Surf Coat Technol 201:371
14. Musiani M (2000) Electrochim Acta 45:3397
15. Gao W, Li Z (2004) Mater Res 7:175
16. Rajagopal I (1983) Bull Mater Sci 5:323
17. Fedorchenko IM, Guslienko YA, Epik AP (1972) Powder Metall Met Ceram 11:626
18. Medeliene V, Leinartas K, Matulionis E (2000) Eur Fed Corro Publ 28:193
19. Bai A, Hu ChCh (2002) Electrochim Acta 47:3447
20. Grande WC, Talbot JB (1993) J Electrochem Soc 140:675
21. Yin KM, Lin BT (1996) Surf Coat Technol 78:205
22. Hessami S, Tobias CW (1989) J Electrochem Soc 136:3611
23. Saraby-Reintjes A, Fleischmann M (1984) Electrochim Acta 29:557
24. Fleischmann M, Saraby-Reintjes A (1984) Electrochim Acta 29:69
25. Proud WG, Gomez E, Sarret E, Valles E, Muller C (1995) J Appl Electrochem 25:770
26. Malpass GRP, Kalaji M, Venancio EC, Motheo AJ (2004) Electrochim Acta 49:4933
27. Shi L, Sun Ch, Gao P, Zhou F, Liu W (2006) Appl Surf Sci 252:3591
28. Wu G, Li N, Zhou D, Mitsuo K (2004) Surf Coat Technol 176:157
29. Srivastava M, Grips VKW, Rajam KS (2007) Appl Surf Sci 253:3814